Proceedings of the ASME 2015 Dynamic Systems and Control Conference
DSCC2015
October 28-30, 2015, Columbus, Ohio, USA

DSCC2015-9622

ENHANCED MOTION CONTROL OF POWERTRAIN USING A COMBINATION OF ACTIVE AND PASSIVE MOUNTS

Jared Liette
The Ohio State University
Columbus, Ohio, USA

Rajendra Singh
The Ohio State University
Columbus, Ohio, USA

ABSTRACT

Vibration control of a realistic coupled powertrain and frame system is analytically and computationally studied using a combination of active and passive mounts. Actuators are placed in the powertrain paths for active control, and passive mounts are employed such that the powertrain roll motion is dominant using the torque roll axis motion decoupling concept. To facilitate this study, a new 24 degree of freedom mathematical model for a coupled powertrain and frame is developed with versatility where passive only, active only, or combined active and passive powertrain paths can be selected. Active control forces are defined as constant, real valued amplitudes to counteract the dominate powertrain roll motion. Alternate path models are then quantitatively compared based on the global powertrain motion magnitudes. It is found that superior vibration control is achieved with combined paths, provided all powertrain paths are aligned with the torque roll axis coordinates. Additionally, successful control is dependent on which paths are selected as a combination of active and passive mounts, dictated by the interaction between active control forces and the passive system dynamics.

INTRODUCTION

Control of rigid body motions and reduction of transmitted (vibratory) forces is commonly accomplished using passive methods [1-11] with adequate success. However, growing consumer expectations (e.g. higher power density) necessitate a hybrid approach of active and passive methods to meet more stringent system design targets, utilizing active control schemes [12-30] and algorithms [31-33] for improved motion and vibration control. Nevertheless, proper hybrid design is application specific and driven by the passive system dynamics, and a quantitative comparison of passive versus hybrid schemes is better facilitated with a specific mounting scheme example, such as for an automotive powertrain. Passive methods such as path isolator designs [1-4] and damping patches [5,6] are traditionally used for vibration isolation and reduction of global motion targets, but there are several practical limitations hindering superior performance [7]. Further, capabilities may be improved through passive physical decoupling of the system motions. For example, proper powertrain mounting system design decouples all rotational and translation motions from the powertrain torque roll axis (TRA) given a torque pulse excitation [8-11]. Yet this introduces additional limitations, such as unrealistic mounting locations and packaging (geometric) space issues [11]. Active control alone also has several limitations: actuator damping is generally low, effecting resonance control capabilities, and stiffness is generally high, increasing system resonances to the audible range and degrading acoustic comfort.

A hybrid approach of active and passive should overcome many limitations of passive or active alone. Studies relevant to powertrain mounting schemes include multiple [12-24] and single [25-29] hybrid path system configurations, where an actuator (active) and rubber or hydraulic element (passive) in series or parallel constitutes a hybrid path. The thrust of prior research is usually on control algorithms, and the passive element is only utilized to provide static support and to ensure the control system stability, though Stewart platforms [19-22] and a tuned reaction mass absorber [23] have been considered. Analysis of passive system dynamics is key in maximizing vibration control performance. Limited relevant studies include Liette et al. [24] quantifying the effect of passive system dynamics on active control capabilities and Park and Singh [25] examining a passive TRA powertrain mounting scheme with one hybrid path. This article expands prior research [24,25] by considering a realistic powertrain mounting scheme which includes frame dynamics [11], aiming for a comparative analysis leading to better design concepts.

PROBLEM FORMULATION

The physical system of this article considers a simplified (yet generic) representation of a typical V6 transverse (east-west) front-engine and transmission with reasonable frame dynamics. The powertrain inertia is approximated as a six degree of freedom rigid body by connecting engine and transmission at an equivalent center of gravity [7], and a four point mounting scheme is assumed. The frame dynamics are also represented by a six degree of freedom rigid body and four point mounting scheme. A planar representation of the system is shown in Fig. 1 for the limiting cases of (a) passive only (Model A) and (b) active only (Model B) powertrain paths, though the frame mounts or bushings are always passive. To examine the effectiveness of a hybrid design, Model C with combined active and passive powertrain paths is considered. In addition to examining various path designs, the effectiveness of passive TRA powertrain mounting paradigms are also studied. Define system configuration 1 as an “arbitrary” mount design (both powertrain and frame mounts are placed at the corners of the respective rigid bodies without any specific design considerations) and configuration 2 as a TRA mount design. All system configurations and corresponding model designations are summarized in Table 1.

The main objective is to quantitatively compare passive, active, and hybrid mounting schemes for vibration control effectiveness. Such a comparison requires formulation of mathematical constructs for all models, and suitable configurations of Models A1 and A2 are already developed by Liette et al. [11]. These models and the corresponding nomenclature are utilized. Discrete linear time-invariant deterministic systems are assumed with small motions, proportional viscous damping, no kinematic nonlinear effects, identical rubber (elastomeric) powertrain and frame mounts with constant properties, and harmonic excitations up to 70 Hz. For low frequencies at steady state system behavior, the rubber mounts are assumed massless. Models B and C require new formulations, and additional assumptions include linear and well known actuators which possess mass. Similar to Liette et al. [24], each actuator input is represented by an applied force at a discrete actuator mass with constant gain. No real-time control is used.

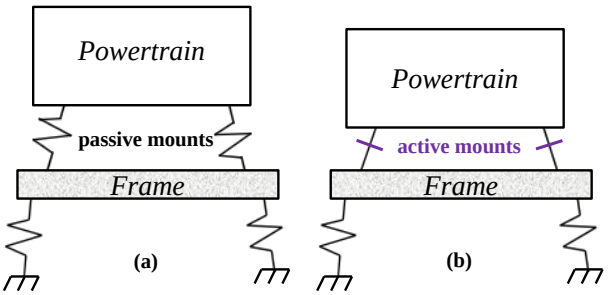

Fig. 1. Limiting cases for powertrain and frame mounting system configurations: (a) passive only and (b) active only.

Table 1. Mounting system configurations and corresponding model designations.

Paths (Mounts)	Model	Configurations
Passive only	A	1, 2
Active only	B	1, 2
Active and Passive	C	1, 2

KEY: 1 – Arbitrary mount design
2 – TRA mount design

Several design issues are investigated as part of the stated objective. For example, only partial TRA decoupling is achievable when frame dynamics are considered [11], which may limit the effectiveness of configuration 2. Also, engine mounts can possess minimal damping for better high frequency performance, degrading resonance control capabilities and limiting effectiveness of the passive paths. The number of active mounts available is a practical concern due to cost and system complexity: one or two is reasonable but all four active paths are not financially viable. This will limit active control effectiveness.

SYSTEM CONFIGURATIONS

Mathematical constructs are first formulated for the models in Table 1 to analyze hybrid path effectiveness. While the schematic and mathematical description of Model A are provided in [11], they are summarized to clarify Model B and C formulations. Model A with passive only powertrain paths is schematically shown in Fig. 2(a). Each rigid body is assumed to have three translational $\boldsymbol{\varepsilon}_{gj} = \left\{ \varepsilon_{gj}^{x} \quad \varepsilon_{gj}^{y} \quad \varepsilon_{gj}^{z} \right\}^{T}$ and three rotational $\boldsymbol{\theta}_{gj} = \left\{ \theta_{gj}^{x} \quad \theta_{gj}^{y} \quad \theta_{gj}^{z} \right\}^{T}$ degrees of freedom in a generalized displacement vector $\mathbf{q}_{gj} = \left\{ \boldsymbol{\varepsilon}_{gj}^{T} \quad \boldsymbol{\theta}_{gj}^{T} \right\}^{T}$. One set of coordinate systems considered are Γ'_{gj} as inertial Cartesian coordinates (x', y', z') at the center of gravity (c.g.) of the j^{th} rigid body. Also, Γ''_{mi} and Γ''_{bi} are principal elastic Cartesian coordinates (x'', y'', z'') of the i^{th} powertrain (subscript m) and frame (subscript b) mount. Lastly, Γ^{TRA} are Cartesian coordinates (x, y, z) where the TRA is the x-axis. All excitation and dynamic reaction forces should eventually be transformed into one coordinate system. Namely, the system should be analyzed in Γ^{TRA} to better facilitate implementation of TRA decoupling [8-11]. Kim [34] has argued that full decoupling is not possible for completely arbitrary mount locations. It is therefore assumed that all mounts are in the so-called mounting plane (x and x'' are parallel), partially decoupling powertrain motions even before seeking appropriate mount locations [9]. Also, all Γ'_{gj} are assumed parallel with a vertical axis and an axis along the driveline.

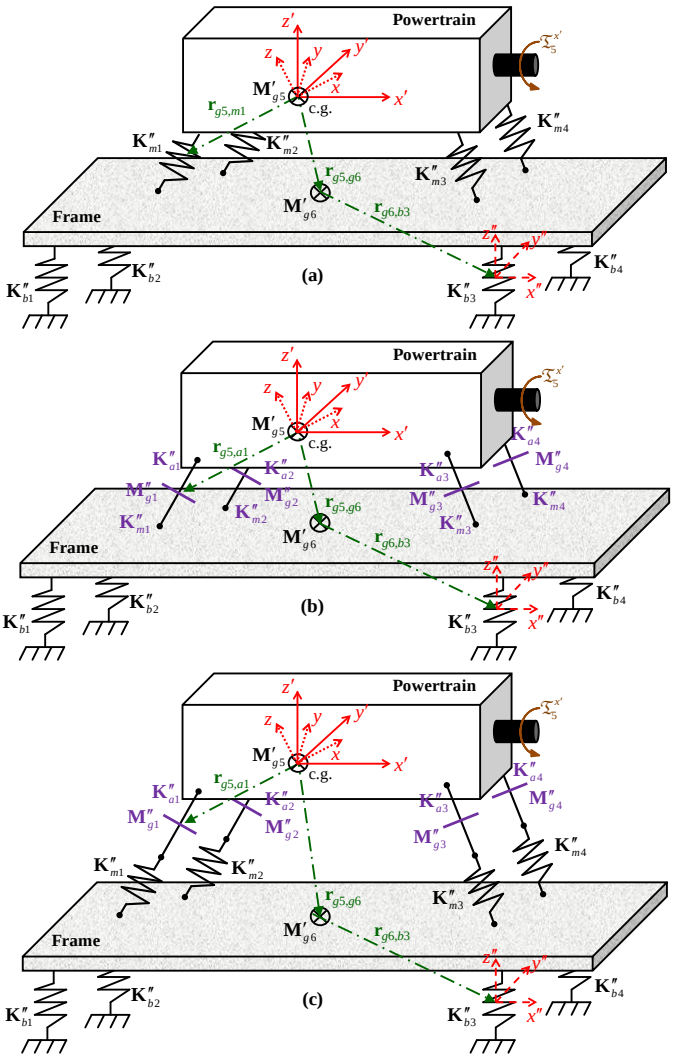

Fig. 2. Schematics for three powertrain and frame mounting system models: (a) Model A, (b) Model B, and (c) Model C.
Key: —, inertial coordinates $\left(\Gamma'_{gj}\right)$; – –, mount coordinates $\left(\Gamma''_{mi}, \Gamma''_{bi}\right)$; and ···, TRA coordinates $\left(\Gamma^{TRA}\right)$.

Inertia properties are $\mathbf{M}'_{g5}$ for the powertrain and $\mathbf{M}'_{g6}$ for the frame in Γ'_{gj} with $\mathbf{M}'_{gj} = \text{diag}\left(\left\{\mathbf{M}'^{\varepsilon}_{gj} \quad \mathbf{M}'^{\theta}_{gj}\right\}\right)$, diag( ) as a diagonal matrix operator, $\mathbf{M}'^{\varepsilon}_{gj} = \text{diag}\left(\left\{m_j \quad m_j \quad m_j\right\}\right)$, m as mass,

$$\mathbf{M}'^{\theta}_{gj} = \begin{bmatrix} I_j^{x'} & -I_j^{x'y'} & -I_j^{x'z'} \\ -I_j^{x'y'} & I_j^{y'} & -I_j^{y'z'} \\ -I_j^{x'z'} & -I_j^{y'z'} & I_j^{z'} \end{bmatrix}, \tag{1}$$

and I as inertia. Stiffness components include the i^{th} powertrain mount $\mathbf{K}''_{mi} = \text{diag}\left(\left\{k_{mi}^{x''} \quad k_{mi}^{y''} \quad k_{mi}^{z''}\right\}\right)$ and $\mathbf{K}''_{bi} = \text{diag}\left(\left\{k_{bi}^{x''} \quad k_{bi}^{y''} \quad k_{bi}^{z''}\right\}\right)$ as the i^{th} frame mount in Γ''_{mi} and Γ''_{bi}, respectively. For a typical elastic mount, torsional stiffnesses are negligible [7], and it is assumed that all mounts are connected to the powertrain and frame by rigid brackets. Position vectors connecting the j^{th} center of gravity to the i^{th} elastic center in Γ^{TRA} are $\mathbf{r}_{gj,mi} = \left\{r_{gj,mi}^{x} \quad r_{gj,mi}^{y} \quad r_{gj,mi}^{z}\right\}^T$ and $\mathbf{r}_{gj,bi} = \left\{r_{gj,bi}^{x} \quad r_{gj,bi}^{y} \quad r_{gj,bi}^{z}\right\}^T$ for the powertrain and frame mounts, respectively. Position vector $\mathbf{r}_{g5,g6} = \left\{r_{g5,g6}^{x} \quad r_{g5,g6}^{y} \quad r_{g5,g6}^{z}\right\}^T$ connects the powertrain and frame centers of gravity, and the system excitation is torque pulse $\mathfrak{T}_5^{x'}(t)$ about the driveline. Except for the powertrain paths, all parameters for Model A are summarized in Table 2(a). These remain unchanged in Models B and C.

Model B with active only powertrain paths, as shown in Fig. 2(b), is modified from Model A by replacing passive powertrain elements with active ones. New symbols include actuator stiffness matrices $\mathbf{K}''_{ai} = \text{diag}\left(\left\{k_{ai}^{x''} \quad k_{ai}^{y''} \quad k_{ai}^{z''}\right\}\right)$ and actuator inertias $\mathbf{M}''_{gj} = \mathbf{M}''^{\varepsilon}_{gj}$, both in Γ''_{mi}. No rotational degrees of freedom are considered for the actuators. Corresponding displacement vectors are $\mathbf{q}_{gj} = \boldsymbol{\varepsilon}_{gj}$ for $i = j =$ 1, 2, 3, 4; and $\mathbf{K}''_{ai}$ account for the internal actuator stiffness and attachment method to the powertrain. Additionally, $\mathbf{K}''_{mi} = \mathbf{K}''_{ai}$ for Model B are roughly an order of magnitude higher than for Model A.

Model C, as shown in Fig. 2(c), has identical notation to Model B. Now, however, the powertrain paths are a hybrid of active and passive elements. Similar to Liette et al. [24], all paths consist of a stiff actuator (attached to the powertrain) in series with a passive rubber elastomer (attached to the frame), as suggested by Beard et al. [35]. A parallel configuration is also commonly done, though a series configuration allows path flexibility for a negligible localized torsional stiffness [7]. Rubber mount stiffness $\mathbf{K}''_{mi}$ and actuator stiffness $\mathbf{K}''_{ai}$ from Models A and B, respectively, are used in Model C. Frame inertia and mount properties in Model A are identical for Models B and C (Examples I and IV from [11] for configurations 1 and 2, respectively).

MATHEMATICAL FORMULATIONS

A discrete mathematical model is first formulated for Model C from Fig. 2(c). To facilitate configuration 2 (TRA mount design), all stiffness and inertia matrices are transformed into Γ^{TRA}. Detailed mathematical analysis in [11] results in $\mathbf{M}_{gj} = \boldsymbol{\Pi}'\mathbf{M}'_{gj}\boldsymbol{\Pi}'^{T}$ for j = 5, 6 (powertrain and frame) where $\boldsymbol{\Pi}' = \text{diag}\left(\left\{\mathfrak{R}' \quad \mathfrak{R}'\right\}\right)$,

$$\mathfrak{R}' = \begin{bmatrix} \upsilon^{xx'} & \upsilon^{xy'} & \upsilon^{xz'} \\ \upsilon^{yx'} & \upsilon^{yy'} & \upsilon^{yz'} \\ \upsilon^{zx'} & \upsilon^{zy'} & \upsilon^{zz'} \end{bmatrix} \tag{2}$$

is a rotational transformation matrix, and υ are normalized directional cosines. Similarly, $\mathbf{K}_{mi} = \mathfrak{R}''_{mi}\mathbf{K}''_{mi}\mathfrak{R}''^{T}_{mi}$ where

$$\mathfrak{R}''_{mi} = \begin{bmatrix} C_{\varphi i}^{y}C_{\varphi i}^{z} & C_{\varphi i}^{x}S_{\varphi i}^{z} + S_{\varphi i}^{x}S_{\varphi i}^{y}C_{\varphi i}^{z} & S_{\varphi i}^{x}S_{\varphi i}^{z} - C_{\varphi i}^{x}S_{\varphi i}^{y}C_{\varphi i}^{z} \\ -C_{\varphi i}^{y}S_{\varphi i}^{z} & C_{\varphi i}^{x}C_{\varphi i}^{z} - S_{\varphi i}^{x}S_{\varphi i}^{y}S_{\varphi i}^{z} & S_{\varphi i}^{x}C_{\varphi i}^{z} + C_{\varphi i}^{x}S_{\varphi i}^{y}S_{\varphi i}^{z} \\ S_{\varphi i}^{y} & -S_{\varphi i}^{x}C_{\varphi i}^{y} & C_{\varphi i}^{x}C_{\varphi i}^{y} \end{bmatrix}. \tag{3}$$

Here, $S_{\varphi i}^{n} = \sin\varphi_{mi}^{n}$ and $C_{\varphi i}^{n} = \cos\varphi_{mi}^{n}$ where n is a general index, and $\boldsymbol{\varphi}_{mi} = \left\{\varphi_{mi}^{x} \quad \varphi_{mi}^{y} \quad \varphi_{mi}^{z}\right\}^T$ are Euler angles from Γ''_{mi} to Γ^{TRA}. Matrix $\mathbf{K}_{mi} = \mathbf{K}_{mi}^{T}$ is generally a fully populated 3x3 matrix, and mounts $\mathbf{K}_{bi} = \mathfrak{R}''_{bi}\mathbf{K}''_{bi}\mathfrak{R}''^{T}_{bi}$ and $\mathbf{K}_{ai} = \mathfrak{R}''_{ai}\mathbf{K}''_{ai}\mathfrak{R}''^{T}_{ai}$ are rotated in the same manner with $\mathfrak{R}''_{ai} = \mathfrak{R}''_{mi}$. Actuator inertia matrices $\mathbf{M}_{gj} = \mathbf{M}''_{gj}$ for j = 1, 2, 3, 4 are diagonal with only translational motions considered. Lastly, powertrain excitation $\mathbf{w}'_{g5}(t) = \left\{0 \quad 0 \quad 0 \quad \mathfrak{T}_5^{x'}(t) \quad 0 \quad 0\right\}^T$ is described as $\mathbf{w}_{g5}(t) = \boldsymbol{\Pi}'\mathbf{w}'_{g5}(t) = \left\{0 \quad 0 \quad 0 \quad \mathfrak{T}_5^{x}(t) \quad \mathfrak{T}_5^{y}(t) \quad \mathfrak{T}_5^{z}(t)\right\}^T$ when rotated into Γ^{TRA} coordinates.

The equations of motion for Model C in Γ^{TRA} are written in compact matrix form as

$$\mathbf{M}_g\ddot{\mathbf{q}}_g(t) + \mathbf{C}_g\dot{\mathbf{q}}_g(t) + \mathbf{K}_g\mathbf{q}_g(t) = \mathbf{w}_g(t) + \mathbf{f}_g(t) \tag{4}$$

with inertia matrix

$$\mathbf{M}_g = \text{diag}\left(\left\{\mathbf{M}_{g1} \quad \mathbf{M}_{g2} \quad \mathbf{M}_{g3} \quad \mathbf{M}_{g4} \quad \mathbf{M}_{g5} \quad \mathbf{M}_{g6}\right\}\right) \tag{5}$$

having 24 degrees of freedom. Define $\mathbf{O}_{nxn}$ as an n x n null matrix, and displacement, disturbance excitation, and control force vectors as

$$\mathbf{q}_g(t) = \left\{\mathbf{q}_{g1}^T(t) \quad \mathbf{q}_{g2}^T(t) \quad \mathbf{q}_{g3}^T(t) \quad \mathbf{q}_{g4}^T(t) \quad \mathbf{q}_{g5}^T(t) \quad \mathbf{q}_{g6}^T(t)\right\}^T, \tag{6}$$

$$\mathbf{w}_g(t) = \left\{\mathbf{O}_{1x3} \quad \mathbf{O}_{1x3} \quad \mathbf{O}_{1x3} \quad \mathbf{O}_{1x3} \quad \mathbf{w}_{g5}^T(t) \quad \mathbf{O}_{1x6}\right\}^T, \tag{7}$$

$$\mathbf{f}_g(t) = \left\{\mathbf{f}_{g1}^T(t) \quad \mathbf{f}_{g2}^T(t) \quad \mathbf{f}_{g3}^T(t) \quad \mathbf{f}_{g4}^T(t) \quad \mathbf{O}_{1x6} \quad \mathbf{O}_{1x6}\right\}^T, \tag{8}$$

respectively. Here, generalized control forces $\mathbf{f}_{gj}(t)$ are applied at the actuators while the disturbance vector $\mathbf{w}_{g5}(t)$ is applied at the powertrain center of gravity. The full stiffness matrix $\mathbf{K}_g$ is symmetric and positive definite with many off-diagonal coupling terms, and a full derivation is shown in Appendix A. Viscous (proportional) damping $\mathbf{C}_g = \mu_1\mathbf{M}_g + \mu_2\mathbf{K}_g$ is defined with Rayleigh coefficients μ_1 and μ_2. Roughly 15% modal damping is assumed with $\mu_1 = \mu_2 = 0.001$.

Table 2
System parameters for (a) powertrain & frame and (b) path models for *i* = *j* = 1, 2, 3, 4.

(a) Powertrain & frame

Parameter	Powertrain	Frame
mass (kg)	$m_5 = 73.2$	$m_6 = 23.9$
inertia (kg m^2)	$\mathbf{M}''^{\theta}_{g5} = \begin{bmatrix} 1.94 & -0.129 & -0.415 \\ -0.129 & 3.43 & 0.073 \\ -0.415 & 0.073 & 3.39 \end{bmatrix}$	$\mathbf{M}''^{\theta}_{g6} = \begin{bmatrix} 3.65 & 0 & 0.027 \\ 0 & 0.678 & 0 \\ 0.027 & 0 & 4.24 \end{bmatrix}$
stiffness (kN mm^{-1})	*	$\mathbf{K}''_{bi} = \text{diag}\left(\{0.67 \quad 0.67 \quad 1.68\}\right)$
position (mm)	$\mathbf{r}_{g5,g6} = \{-166 \quad 54 \quad -548\}^T$	--

*Powertrain mount stiffnesses depend on path models

(b) Path models for *i* = *j* = 1, 2, 3, 4

Parameter	Passive	Active	Active + Passive
m_j (kg)	0.002	2	2
$\mathbf{K}''_{mi}$ (kN mm^{-1})	$\text{diag}\left(\{0.34 \quad 0.34 \quad 0.84\}\right)$	$\text{diag}\left(\{2.80 \quad 2.80 \quad 5.60\}\right)$	$\text{diag}\left(\{0.34 \quad 0.34 \quad 0.84\}\right)$
$\mathbf{K}''_{ai}$ (kN mm^{-1})	$\text{diag}\left(\{2800 \quad 2800 \quad 5600\}\right)$	$\text{diag}\left(\{2.80 \quad 2.80 \quad 5.60\}\right)$	$\text{diag}\left(\{2.80 \quad 2.80 \quad 5.60\}\right)$
μ_1 (--)	0.001	0.001	0.001
μ_2 (--)	0.001	0.0001	0.001
$\ell^{z''}_{gj,mi}$ (mm)	0	5	10
$\ell^{z''}_{gj,ai}$ (mm)	0	5	5

To enhance its versatility, the formulation for Model C is also used for Models A and B with appropriate path modifications. All $\mathbf{r}_{g5,mi}$ are defined in [11] for both arbitrary (Example I in [11]) and TRA (Example IV in [11]) mount designs. Models A1 and A2 use these values. Assuming powertrain and frame rigid bodies remain in the same spatial coordinates for all models, a kinematic relationship between $\mathbf{r}_{g5,ai}$ and $\mathbf{r}_{g5,mi}$ is illustrated in Fig. 3. The result is an adjusted $r^{z''}_{g5,ai} = r^{z''}_{g5,mi} + \ell^{z''}_{gj,mi} + \ell^{z''}_{gj,ai}$. Other components of the position vector $r^{x''}_{g5,ai} = r^{x''}_{g5,mi}$ and $r^{y''}_{g5,ai} = r^{y''}_{g5,mi}$ remain unchanged in the local mount coordinates. The position vectors are then rotated into TRA coordinates as $\mathbf{r}_{g5,mi} = \mathfrak{R}''_{mi}\mathbf{r}''_{g5,mi}$ and $\mathbf{r}_{g5,ai} = \mathfrak{R}''_{ai}\mathbf{r}''_{g5,ai}$.

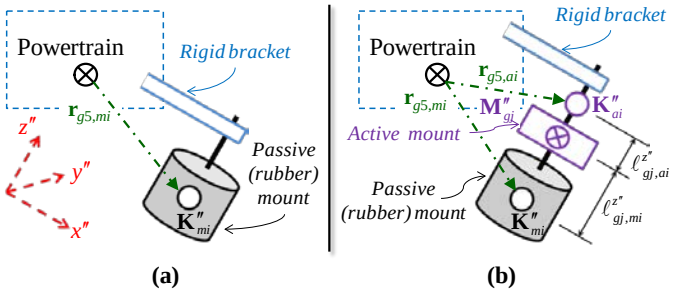

Fig. 3. Kinematic relationship between path configurations: (a) with passive mounts only and (b) with active and passive mounts.

Thus, $\mathbf{r}_{g5,ai}$ is defined for Model C by assigning reasonable values of $\ell^{z''}_{gj,mi} = 10$ mm and $\ell^{z''}_{gj,ai} = 5$ mm, assuming the rubber mount is thicker than the actuator. Similarly, $\ell^{z''}_{gj,mi} = \ell^{z''}_{gj,ai} = 5$ mm for Model B assuming symmetric actuator attachment points from the center of gravity. Modifications also must be made to the actuator properties $\mathbf{M}''_{gj}$, $\mathbf{K}''_{mi}$,and $\mathbf{K}''_{ai}$. Transitioning from Model C to B only needs $\mathbf{K}''_{mi} = \mathbf{K}''_{ai}$ and $\mu_2 = 0.0001$ as the changes (roughly 1.5% modal damping with only actuators). Transitioning from Model C to A requires the actuator dynamics to be made negligible. This is achieved with $\hat{m}_j = m_j/1000$ and $\hat{\mathbf{K}}''_{ai} = 1000\mathbf{K}''_{ai}$ as active path elements modified to represent passive ones, resulting in $\mathbf{K}''_{mi}$ dominating path dynamics at low frequencies. Parameters for the path models are summarized in Table 2(b), and all configurations in Table 1 are now fully defined.

COMPARATIVE STUDY OF CONFIGURATIONS

Next, a quantitative comparison of passive, active, and hybrid mounting scheme paradigms for vibration control effectiveness is conducted by comparing global powertrain motion magnitudes (on a dB basis) up to 70 Hz. First, consider Model A1 (passive only, arbitrary mount design) and Model A2 (passive only, TRA mount design). Powertrain and frame mount locations are taken from Examples I and IV in [11], respectively, and approximate powertrain mount locations are illustrated in Fig. 4. Note that Example IV in [11] designs both powertrain and frame mounts using TRA principles, and (more realistic) parameters when powertrain and frame TRA do not align are used in Model A2. Position of frame mount #2 is also adjusted from an unrealistic $r^{z'}_{g6,b2} = 1090$ mm calculated in [11] to a more reasonable $r^{z'}_{g6,b2} = 200$ mm. It is assumed that all paths are oriented in the so-called mounting plane (x and x'' are parallel) with

$\varphi^y_{mi} = \varphi^z_{mi} = 0$, and only a rotation of φ^x_{mi} is needed to transform from Γ''_{mi} to Γ^{TRA} [9]. Mount orientation angles of $\varphi^x_{mi} = \pm 30°$ and $\varphi^x_{bi} = \pm 10°$ are used, pitching the mounts inward to support the powertrain and frame bodies.

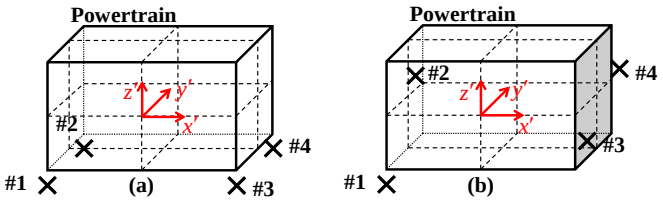

Fig. 4. Mount (path) locations (marked by X) relative to the powertrain (rigid body) for (a) "arbitrary" design and (b) TRA design.

Powertrain motions for Model A1 with nominal mount damping (resonance control), Model A1 with minimal damping (about 3% modal damping), and Model A2 are compared in Fig. 5(a). Note that the dynamic range (60 dB) is very large, and anything beyond that would represent the computational noise floor. Minimal damping results in much higher peaks than resonance control type damping with maximum $\left|\varepsilon^y_{g5}\right|$ reaching 20 dB, leading to undesirable performance. Hence, the nominal damping of Model A and Model C (with passive path components) is selected for resonance control. The TRA design of Model A2 yields good partial decoupling between the roll motion $\left|\theta^x_{g5}\right|$ and all other powertrain motions, though significant motion does occur in the $\left|\varepsilon^y_{g5}\right|$ translational direction. Additionally, the designed TRA mode at resonance frequency $\Omega^{TRA}/2\pi = 32$ Hz is prominent in $\left|\theta^x_{g5}\right|$. New TRA mount locations may be difficult to implement given packaging space concerns, but overall motion levels are much lower than the arbitrary mount design of Model A1.

Model B1 (active only, arbitrary mount design) and Model B2 (active only, TRA mount design) are compared in Fig. 5(b) with no control forces applied. Though the paths are much stiffer, the TRA design of [11] yields similar mount locations. However, the TRA mode at $\Omega^{TRA}/2\pi = 63$ Hz in $\left|\theta^x_{g5}\right|$ is at a higher frequency, and the lower damping provides no resonance control. This illustrates why active control alone is not utilized in practice for such a system, where all motions cannot be reduced to zero given a limited number of actuators and with significant coupling in the stiffness matrix. A passive mount (in series or parallel hybrid configuration) is necessary to provide adequate damping for uncontrolled modes that are excited.

It has been demonstrated that the passive TRA mount design yields lower overall powertrain motions, and this holds true for Model C. Results for Model C1 are therefore not shown as they provide no additional insight. Instead, a comparison is done between Model A2 and Model C2, as included actuator dynamics may have an adverse effect on partial TRA decoupling effectiveness. This comparison is shown in Fig. 6, and TRA partial decoupling is indeed still effective for Model C2 (paths #1 and #2 are hybrid). The TRA roll mode is evident at $\Omega^{TRA}/2\pi = 29$ Hz in $\left|\theta^x_{g5}\right|$, and the magnitude spectra in general are similar to Model A2. The main difference is an increase in $\left|\varepsilon^z_{g5}\right|$ and $\left|\theta^z_{g5}\right|$ due to actuator mass participation, but $\left|\theta^x_{g5}\right|$ still dominates over most frequencies.

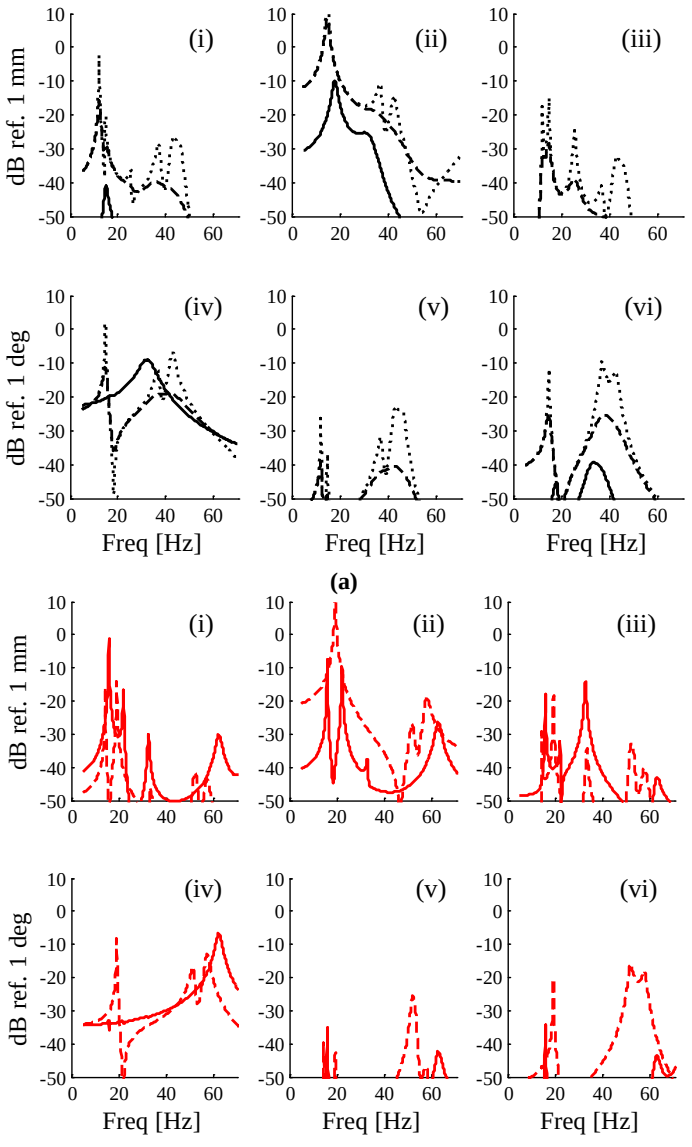

Fig. 5. Powertrain motion (magnitude) spectra for (i) $\left|\varepsilon^x_{g5}\right|$, (ii) $\left|\varepsilon^y_{g5}\right|$, (iii) $\left|\varepsilon^z_{g5}\right|$, (iv) $\left|\theta^x_{g5}\right|$, (v) $\left|\theta^y_{g5}\right|$, and (vi) $\left|\theta^z_{g5}\right|$ for alternate models: (a) Model A and (b) Model B. Key: (a) − −, Model A1; ⋯, Model A1 with low damping; —, Model A2 and (b) − −, Model B1; —, Model B2.

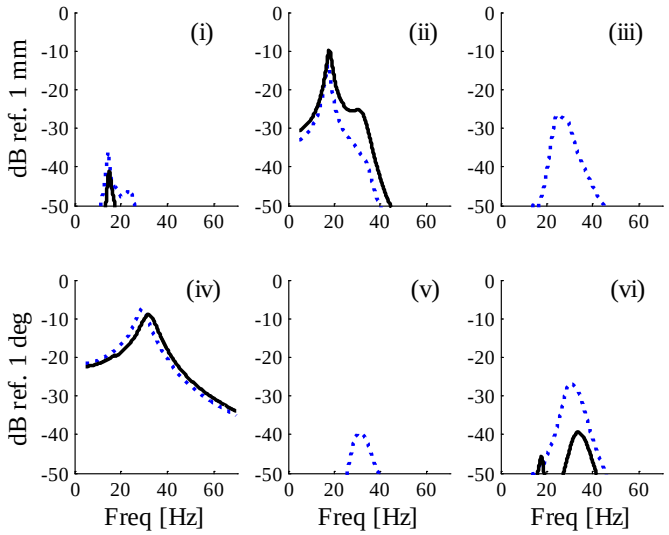

Fig. 6. Comparison of Model A2 and Model C2 (paths #1 and #2 hybrid) powertrain motion (magnitude) spectra: (i) $\left|\varepsilon_{g5}^{x}\right|$, (ii) $\left|\varepsilon_{g5}^{y}\right|$, (iii) $\left|\varepsilon_{g5}^{z}\right|$, (iv) $\left|\theta_{g5}^{x}\right|$, (v) $\left|\theta_{g5}^{y}\right|$, and (vi) $\left|\theta_{g5}^{z}\right|$. Key: —, Model A2 and ···, Model C2.

MOTION CONTROL USING HYBRID PATHS

Hybrid control capabilities are now explored by applying active control forces to the hybrid paths in Model C2. The number of actuators used is a practical concern due to cost, and this study is limited to only two hybrid paths. It has already been demonstrated by Park and Singh [25] that one hybrid path is not sufficient. Analysis is done in the frequency domain, and complex valued parameters are defined as $\tilde{w}_n(t) = W_n e^{i\omega t}$, $\tilde{f}_n(t) = \tilde{\mathcal{F}}_n e^{i\omega t}$, and $\tilde{q}_n(t) = \tilde{Q}_n e^{i\omega t}$ where n is a general index, ω is the excitation frequency in rad sec^{-1}, $i = \sqrt{-1}$, W_n is the disturbance excitation amplitude with zero reference phase for disturbance excitation $\tilde{w}_n(t)$, $\tilde{\mathcal{F}}_n$ is the complex valued control force amplitude for control force $\tilde{f}_n(t)$, and $\tilde{Q}_n$ is the complex valued displacement amplitude for displacement $\tilde{q}_n(t)$. Equations of motion are then re-written as

$$\left[-\omega^2\mathbf{M}_g + i\omega\mathbf{C}_g + \mathbf{K}_g\right]\tilde{\mathbf{Q}}_g e^{i\omega t} = \left\{\mathbf{W}_g + \tilde{\mathbf{F}}_g\right\} e^{i\omega t} \tag{9}$$

where $\tilde{\mathbf{Q}}_g$, $\mathbf{W}_g$, and $\tilde{\mathbf{F}}_g$ are vectors of displacement, disturbance, and control force amplitudes, respectively. The disturbance torque amplitudes $\mathbf{W}_{g5} = \{0 \;\; 0 \;\; 0 \;\; T_5^x \;\; T_5^y \;\; T_5^z\}^T$ excite the powertrain where $\tilde{\mathfrak{T}}_n(t) = T_n e^{i\omega t}$. Finally, $\tilde{\mathbf{Q}}_g = \tilde{\mathbf{H}}_g\left\{\mathbf{W}_g + \tilde{\mathbf{F}}_g\right\}$ is solved where $\tilde{\mathbf{H}}_g = \left[-\omega^2\mathbf{M}_g + i\omega\mathbf{C}_g + \mathbf{K}_g\right]^{-1}$ is the complex valued compliance matrix.

Before calculating $\tilde{\mathbf{Q}}_g$ from the system equations of motion, the control forces must be defined in the Γ^{TRA} coordinates. It is assumed that all actuators apply only axial forces in the z''-direction such that $\tilde{\mathbf{F}}''_{gj} = \{0 \;\; 0 \;\; \tilde{\mathcal{F}}''_j\}^T$. Assuming the path is oriented in the so-called mounting plane (x and x'' are parallel) with $\varphi_{mi}^y = \varphi_{mi}^z = 0°$, a rotation of φ_{mi}^x only is needed to transform from Γ''_{mi} to Γ^{TRA} [9]. Then,

$$\tilde{\mathbf{F}}_{gj} = \mathfrak{R}''_{mi}\tilde{\mathbf{F}}''_{gj} = \begin{bmatrix} 1 & 0 & 0 \\ 0 & C_{\varphi i}^x & S_{\varphi i}^x \\ 0 & -S_{\varphi i}^x & C_{\varphi i}^x \end{bmatrix}\begin{Bmatrix} 0 \\ 0 \\ \tilde{\mathcal{F}}''_j \end{Bmatrix} \tag{10}$$

results in $\tilde{\mathbf{F}}_{gj} = \{0 \;\; S_{\varphi i}^x\tilde{\mathcal{F}}''_j \;\; C_{\varphi i}^x\tilde{\mathcal{F}}''_j\}^T = \{0 \;\; \tilde{\mathcal{F}}_j^y \;\; \tilde{\mathcal{F}}_j^z\}^T$. Thus, the system is excited in two translational directions (y and z) by each control force.

Detailed closed loop control forces calculations are not done, nor are real time control strategies. Instead, the control forces for hybrid paths #1 and #2 are selected as $\mathcal{F}_1'' = -\mathcal{F}_2''$ to counteract the dominate powertrain roll motion θ_{g5}^x. These force amplitudes are assumed real valued and constant for all ω. This allows for a simplified study to demonstrate the feasibility of hybrid powertrain vibration control for improved performance, combining passive TRA motion decoupling with active motion control. The results for model C2 are shown in Fig. 7(a). A restricted dynamic range of -50 to 0 dB is shown for a consistent comparison and sufficient detail in all active control plots, though $\left|\varepsilon_{g5}^y\right|$ does have a peak greater than 0 dB. Significant attenuation is achieved in $\left|\theta_{g5}^x\right|$, with a max reduction of 12 dB and a reduction of 5 dB at Ω^{TRA}. Results vary depending on the value of $\mathcal{F}_1''$ selected. However, large increases occur in all other powertrain motions, and the overall vibration control performance is worse. The path orientations are $\varphi_{mi}^x = \pm 30°$ for this example case, exciting both the y and z translational directions. This likely causes the observed detrimental effect in vibration control.

Better results may be achieved if $\varphi_{mi}^x = 0°$ are selected, as only the z translational direction would be excited. This, however, could be problematic for static support of the powertrain. Coordinates Γ^{TRA} and Γ'_{gj} do not coincide for a realistic powertrain with an asymmetric inertia matrix, deviating by as much as 25° in many practical cases [36], and $\varphi_{mi}^x = 0°$ therefore does not imply vertically oriented mounts. Regardless, it is worthwhile to investigate as part of this feasibility study, and the results are shown in Fig. 7(b). The same $\mathcal{F}_1''$ value used for $\varphi_{mi}^x = \pm 30°$ is selected. In this case, the dominate roll motion is attenuated even more, with a consistent reduction of about 10 dB. Additionally, the other powertrain motions are either reduced or not strongly amplified across the frequency range of interest. The exception is a peak at about 14 Hz in $\left|\varepsilon_{g5}^x\right|$. This demonstrates the feasibility of improving powertrain vibration control using a hybrid approach of passive TRA motion decoupling combined with active motion control, as opposed to using passive or active methods only. It is also noted that the powertrain motions with no applied control forces are slightly different between the $\varphi_{mi}^x = \pm 30°$ and $\varphi_{mi}^x = 0°$ cases. Still, the roll motion $\left|\theta_{g5}^x\right|$ dominates most of the frequency spectra in both.

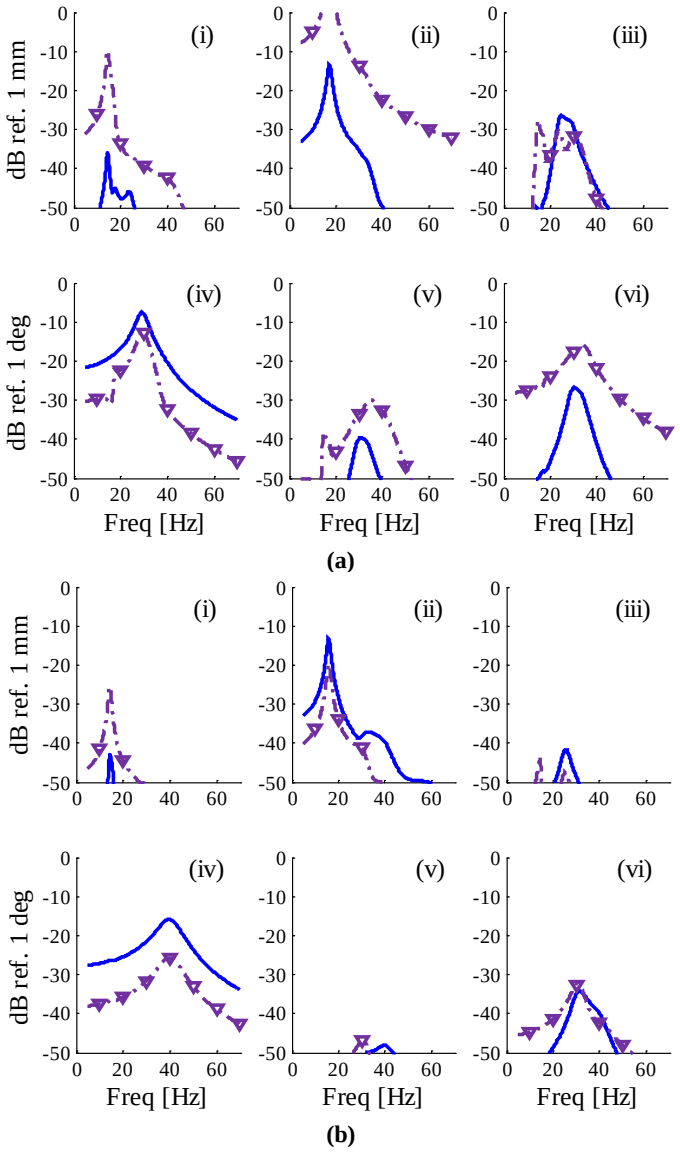

Fig. 7. Comparison of Model C2 (hybrid paths #1 and #2) powertrain motion (magnitude) spectra (i) $|\varepsilon_{g5}^{x}|$, (ii) $|\varepsilon_{g5}^{y}|$, (iii) $|\varepsilon_{g5}^{z}|$, (iv) $|\theta_{g5}^{x}|$, (v) $|\theta_{g5}^{y}|$, and (vi) $|\theta_{g5}^{z}|$ with and without applied control forces for alternate path orientations (a) $\varphi_{mi}^{x} = \pm 30°$ and (b) $\varphi_{mi}^{x} = 0°$. Key: —, no applied control forces and –·▽·–, applied control forces.

The successful hybrid control results of Model C2 are next compared to Model B2 (active only) in Fig. 8. The same $\mathcal{F}_1''$ is used and $\varphi_{mi}^{x} = 0°$ for all paths. Additionally, the frequency range is from 0 to 100 Hz to capture the roll motion peak in Model B2, and active control forces are applied in paths #1 and #2. The motion magnitudes in Model B2 are generally much larger, especially in the lateral motions where increases of 23 dB, 11 dB, and 25 dB are observed in $|\varepsilon_{g5}^{x}|$, $|\varepsilon_{g5}^{y}|$, and $|\varepsilon_{g5}^{z}|$ peak motions, respectively. This further confirms the need for some passive control, accomplished with the hybrid path configuration. The roll motion $|\theta_{g5}^{x}|$ is lower for Model B2, though the peak is at a much higher frequency. Similar results are obtained for the other configurations of Model C2 that have been examined.

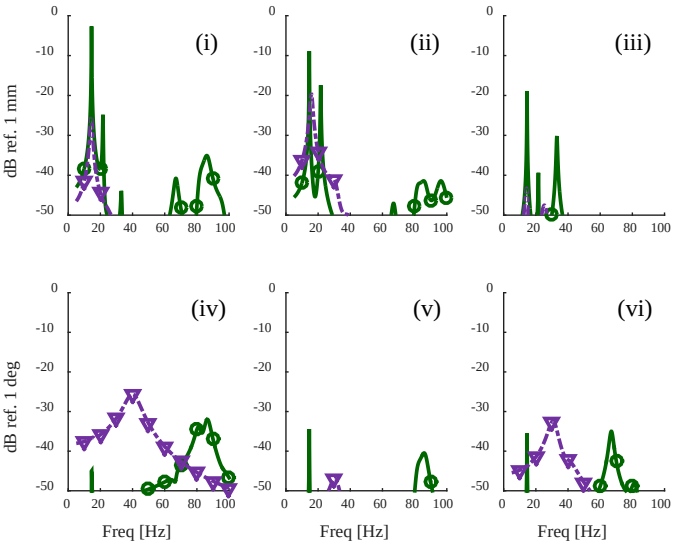

Fig. 8. Comparison of Model B2 and Model C2 (active paths #1 and #2, $\varphi_{mi}^{x} = 0°$) powertrain motion (magnitude) spectra (i) $|\varepsilon_{g5}^{x}|$, (ii) $|\varepsilon_{g5}^{y}|$, (iii) $|\varepsilon_{g5}^{z}|$, (iv) $|\theta_{g5}^{x}|$, (v) $|\theta_{g5}^{y}|$, and (vi) $|\theta_{g5}^{z}|$. Key: —○—, Model B2 and –·▽·–, Model C2.

Though successful results are obtained with hybrid paths #1 and #2 in Model C2, using a different combination of hybrid paths may yield unacceptable magnitudes for the non-targeted powertrain motions. For example, consider using hybrid paths #1 and #4 with $\mathcal{F}_1'' = -\mathcal{F}_4''$ being the same magnitude as the previous cases. This is shown in Fig. 9. Significant attenuation of roll motion $|\theta_{g5}^{x}|$ is again achieved, but several powertrain motions are amplified to very high levels. This illustrates the impact of the passive system dynamics on active control effectiveness. A similar concept is demonstrated by Liette et al. [24] for a simplified powertrain and frame system with only two paths, and the system compliance matrix $\tilde{\mathbf{H}}$ dictates control effectiveness.

The system eigenvectors may yield some insight into which path combinations give superior results, as they contain information about the inherent passive coupling within the system. For example, define

$$\bar{v}_n = \left\{ \varepsilon_{g5}^{x} \quad \varepsilon_{g5}^{y} \quad \varepsilon_{g5}^{z} \quad \theta_{g5}^{x} \quad \theta_{g5}^{y} \quad \theta_{g5}^{z} \right\} \tag{11}$$

as the normalized eigenvector corresponding to the powertrain motions for mode *n*. Model C2 with hybrid paths #1 and #2 (successful case) yields

$$\bar{v}_3 = \left\{ 0.110 \quad -0.001 \quad 1.000 \quad -0.0290 \quad -0.162 \quad 0.040 \right\} \tag{12}$$

as the mode 3 eigenvector (about 25 Hz). This mode is dominated by $|\varepsilon^z_{g5}|$ with coupling to all other powertrain motions. Now consider Model C2 with hybrid paths #1 and #4 (unsuccessful case), where

$$\bar{v}_3 = \{0.133 \quad -0.001 \quad 1.000 \quad -0.0434 \quad -0.452 \quad 0.101\} \qquad (13)$$

is the mode 3 eigenvector. The coupling to all rotational motions has greatly increased, including the targeted roll motion $|\theta^x_{g5}|$. Additionally, a hybrid combination of #1 and #4 with out-of-phase control forces excites $|\theta^y_{g5}|$ much more than a combination of #1 and #2 (evident from Fig. 4), as the forces are additive in the former but counteract each other in the latter. Coupling to $|\theta^y_{g5}|$ has greatly increased in $\bar{v}_3$, and the vertical motion therefore greatly increases. Further detailed analysis of this coupling effect for Model C2 is left to future work.

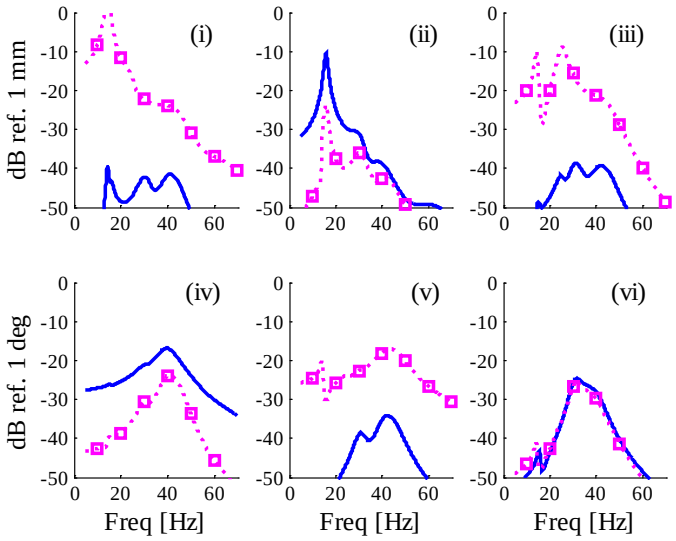

Fig. 9. Model C2 (hybrid paths #1 and #4, $\varphi^x_{mi} = 0°$) powertrain motion (magnitude) spectra (i) $|\varepsilon^x_{g5}|$, (ii) $|\varepsilon^y_{g5}|$, (iii) $|\varepsilon^z_{g5}|$, (iv) $|\theta^x_{g5}|$, (v) $|\theta^y_{g5}|$, and (vi) $|\theta^z_{g5}|$ with and without applied control forces. Key: —, no applied control forces and —□—, applied control forces.

CONCLUSION

The main contribution of this study is the demonstration of improved powertrain vibration control with a hybrid (active and passive) mounting scheme over active or passive only. For the hybrid approach, passive TRA partial motion decoupling is combined with active powertrain motion control, causing the powertrain roll motion to dominate and then counteracting this motion with the control forces. To facilitate this contribution, a new mathematical model is derived for a coupled powertrain and frame with versatility to allow passive only, active only, or hybrid powertrain paths to be selected with arbitrary or TRA designed mount locations. This new versatile model is also a contribution, aiming towards future vehicle models considering frame dynamics and hybrid paths. The mount orientations are found to be of critical importance, and inferior results are obtained if $\varphi^x_{mi} = \pm 30°$ are selected. Orientations of $\varphi^x_{mi} = 0^\circ$ yield superior results, though this may cause issues with static support of the powertrain body. The paths selected to be hybrid are also significant. Using paths #1 and #2 yield superior results, while using paths #1 and #4 has a detrimental effect on non-targeted powertrain motions. This illustrates the influence of passive system dynamics on the vibration control effectiveness, and a detailed investigation should be conducted as part of future research.

ACKNOWLEDGMENTS

We acknowledge the member organizations of the Smart Vehicle Concepts Center (www.SmartVehicleCenter.org) and the National Science Foundation Industry/University Cooperative Research Centers program (www.nsf.gov/eng/iip/iucrc) for supporting this basic research.

REFERENCES

[1] Inoue, A., Singh, R., and Fernandes, G. A., 2008, "Absolute and Relative Path Measures in a Discrete System by Using Two Analytical Methods," Journal of Sound and Vibration 313, pp. 696-722.

[2] Kim, S. and Singh, R., 2001, "Multi-Dimensional Characterization of Vibration Isolators Over a Wide Range of Frequencies," J. of Sound and Vibration, 245(5), pp. 877-913.

[3] Ibrahim, R. A., 2008, "Recent Advances in Nonlinear Passive Vibration Isolators," J. of Sound and Vibration, 314, pp. 371-452.

[4] Den Hartog, J. P., 1985, Mechanical Vibrations, Dover Publications, New York, USA.

[5] Kung, S. W. and Singh, R., 1998, "Vibration Analysis of Beams with Multiple Constrained Layer Damping Patches," J. of Sound and Vibration, 212(5), pp. 781-805.

[6] Kung, S. W. and Singh, R., 1999, "Development of Approximate Methods for the Analysis of Patch Damping Concepts," J. of Sound and Vibration, 219(5), pp. 785-812.

[7] Harris, C. M., 1995, Shock and Vibration Handbook, McGraw-Hill, New York, USA.

[8] Hu, J.-F. and Singh, R., 2012, "Improved Torque Roll Axis Decoupling Axiom for a Powertrain Mounting System in the Presence of a Compliant Base," J. of Sound and Vibration, 331(7), pp. 1498–1518.

[9] Jeong, T. and Singh, R., 2000, "Analytical Methods of Decoupling the Automotive Engine Torque Roll Axis," J. of Sound and Vibration, 234(1), pp. 85-114.

[10] Park, J.-Y. and Singh, R., 2008, "Effect of Non-Proportional Damping on the Torque Roll Axis Decoupling of an Engine Mounting System," J. of Sound and Vibration, 313, pp. 841-857.

[11] Liette, J., Dreyer, J. T., and Singh, R., 2014, "Critical Examination of Isolation System Design Paradigms for a Coupled Powertrain and Frame: Partial Torque Roll Axis Decoupling Methods Given Practical Constraints," J. of Sound and Vibration, 333, pp. 7089-7108.

[12] Serrand, M. and Elliott, S. J., 2000, "Multichannel Feedback Control of the Isolation of Base-Excited Vibration," J. of Sound and Vibration, 234(4), pp. 681-704.

[13] Huang, X., Elliott, S. J., and Brennan, M. J., 2003, "Active Isolation of a Flexible Structure from Base Vibration," J. of Sound and Vibration, 263, pp. 357-376.

[14] Yang, T. J., Suai, Z. J., Sun, Y., Shu, M. G., Xiao, Y. H., Liu, X. G., Du, J. T., Jin, G. Y., and Liu, Z. G., 2012, "Active Vibration Isolation System for a Diesel Engine," Noise Control Engineering J., 60(3), pp. 267-282.

[15] Gardonio, P. and Elliott, S. J., 2000, "Passive and Active Isolation of Structural Vibration Transmission Between Two Plates Connected by a Set of Mounts," J. of Sound and Vibration, 237(3), pp. 483-511.

[16] Kim, S. M., Elliott, S. J., and Brennan, M. J., 2001, "Decentralised Control for Multichannel Active Vibration Isolation," IEEE Transactions on Control Systems Technology, 9(1), pp. 93-100.

[17] Gardonio, P., Elliott, S. J., and Pinnington, R. J., 1997, "Active Isolation of Structural Vibration on a Multiple-Degree-of-Freedom System, Part I: The Dynamics of the System," J. of Sound and Vibration, 207(1), pp. 61-93.

[18] Gardonio, P., Elliott, S. J., and Pinnington, R. J., 1997, "Active Isolation of Structural Vibration on a Multiple-Degree-of-Freedom System, Part II: Effectiveness of Active Control Strategies," J. of Sound and Vibration, 207(1), pp. 95-121.

[19] Geng, Z. J. and Haynes, L. S., 1994, "Six Degree-of-Freedom Active Vibration Control Using the Stewart Platforms," IEEE Transactions on Control Systems Technology, 2(1), pp. 45-53.

[20] Preumont, A., Horodinca, M., Romanescu, I., Marneffe, B. de, Avraam, M., Deraemaeker, A., Bossens, F., and Hanieh, A. Abu, 2007, "A Six-Axis Single-Stage Active Vibration Isolator Based on Stewart Platform," J. of Sound and Vibration, 300, pp. 644-661.

[21] Stewart, D., 1965, "A Platform with Six Degrees of Freedom," Proceedings of the Institute of Mechanical Engineers, 180(1), pp. 371-386.

[22] Preumont, A., 2002, Vibration Control of Active Structures, An Introduction, Kluwer Academic Publishers, Massachusetts, USA.

[23] Garcia, E., Webb, S., and Duke, J., 1995, "Passive and Active Control of a Complex Flexible Structure Using Reaction Mass Actuators," J. of Vibration and Acoustics, 117, pp. 116-122.

[24] Liette, J., Dreyer, J. T., and Singh, R., 2014, "Interaction Between Two Active Structural Paths for Source Mass Motion Control Over Mid-Frequency Range," J. of Sound and Vibration, 333, pp. 2369-2385.

[25] Park, J.-Y. and Singh, R., 2009, "Analysis of Powertrain Motions Given a Combination of Active and Passive Isolators," Noise Control Engineering J., 57(3), pp. 232-243.

[26] Kim, B., Washington, G. N., and Singh, R., 2012, "Control of Modulated Vibration Using and Enhanced Adaptive Filtering Algorithm Based on Model-Based Approach," J. of Sound and Vibration, 331, pp. 4101-4114.

[27] Kim, B., Washington, G. N., and Singh, R., 2012, "Control of Incommensurate Sinusoids Using Enhanced Adaptive Filtering Algorithm Based on Sliding Mode Approach," J. of Vibration and Control, 19(8), pp. 1265-1280.

[28] Pinte, G., Devos, S., Stallaert, B., Symens, W., Swevers, J., and Sas., P., 2010, "A Piezo-Based Bearing for the Active Structural Acoustic Control of Rotating Machinery," J. of Sound and Vibration, 329, pp. 1235-1253.

[29] Elliott, S. J., 1994, "Active Control of Structure-Borne Noise," J. of Sound and Vibration, 177(5), pp. 651-673.

[30] Fakhari, V. and Ohadi, A., 2012, "Robust Control of Automotive Engine Using Active Engine Mount," J. of Vibration and Control, 19(7), pp. 1024-1050.

[31] Elliott, S. J., 2008, "A Review of Active Noise and Vibration Control in Road Vehicles," ISVR Technical Memorandum, 981, pp. 1-25.

[32] Alkhatib, R. and Golnaraghi, M. F., 2003, "Active Structural Vibration Control: A Review," The Shock and Vibration Digest, 35(5), pp. 367-383.

[33] Fuller, C. R., Elliott, S. J., and Nelson, P. A., 1996, Active Control of Vibration, Academic Press Inc., California, USA.

[34] Kim, B. J., 1991, "Three Dimensional Vibration Isolation Using Elastic Axes," M.S. Thesis, Michigan State University, MI.

[35] Beard, M. J., Von Flotow, A. H., and Schubert, D. W., 1994, "A Practical Product Implementation of an Active/Passive Vibration Isolation System," Proceedings of IUTAM symposium on the Active Control of Vibration, University of Bath, UK, pp. 101-108.

[36] Brach, R. M., 1997, "Automotive Powerplant Isolation Strategies," SAE Paper No. 971942.

APPENDIX A: DERIVATION OF STIFFNESS MATRIX

For the actuator rigid bodies, $\mathbf{K}_{gj} = \mathbf{K}_{ai} + \mathbf{K}_{mi}$ for $i = j = 1, 2, 3, 4$. The combined stiffness of all mounts as well as torsional effects, as applicable to powertrain and frame bodies, is expressed as

$$\mathbf{K}_{g5} = \begin{bmatrix} \sum_{i=1}^{4} \mathbf{K}_{ai} & \sum_{i=1}^{4} \mathbf{K}_{ai}\mathbf{E}_{g5,ai} \\ \sum_{i=1}^{4} \left(\mathbf{K}_{ai}\mathbf{E}_{g5,ai}\right)^T & \sum_{i=1}^{4} \left(\mathbf{E}_{g5,ai}\right)^T \mathbf{K}_{ai}\mathbf{E}_{g5,ai} \end{bmatrix} = \begin{bmatrix} \mathbf{K}_{g5}^{11} & \mathbf{K}_{g5}^{12} \\ \mathbf{K}_{g5}^{21} & \mathbf{K}_{g5}^{22} \end{bmatrix}, \quad \text{(A.1)}$$

$$\mathbf{K}_{g6} = \begin{bmatrix} \sum_{i=1}^{4} \mathbf{K}_{mi} & \sum_{i=1}^{4} \mathbf{K}_{mi}\mathbf{E}_{g6,mi} \\ \sum_{i=1}^{4} \left(\mathbf{K}_{mi}\mathbf{E}_{g6,mi}\right)^T & \sum_{i=1}^{4} \left(\mathbf{E}_{g6,mi}\right)^T \mathbf{K}_{mi}\mathbf{E}_{g6,mi} \end{bmatrix} = \begin{bmatrix} \mathbf{K}_{g6}^{11} & \mathbf{K}_{g6}^{12} \\ \mathbf{K}_{g6}^{21} & \mathbf{K}_{g6}^{22} \end{bmatrix}. \quad \text{(A.2)}$$

Derivations are included in [11] where $\mathbf{E}$ is a skew symmetric matrix consisting of position vector components. The full system stiffness matrix is constructed as $\mathbf{K}_g = \begin{bmatrix} \mathbf{K}_g^{11} & -\mathbf{K}_g^{12}; & -\mathbf{K}_g^{21} & \mathbf{K}_g^{22} \end{bmatrix}$ where

$$\mathbf{K}_g^{11} = \begin{bmatrix} \mathbf{K}_{g1} & \mathbf{O}_{3x3} & \mathbf{O}_{3x3} & \mathbf{O}_{3x3} \\ \mathbf{O}_{3x3} & \mathbf{K}_{g2} & \mathbf{O}_{3x3} & \mathbf{O}_{3x3} \\ \mathbf{O}_{3x3} & \mathbf{O}_{3x3} & \mathbf{K}_{g3} & \mathbf{O}_{3x3} \\ \mathbf{O}_{3x3} & \mathbf{O}_{3x3} & \mathbf{O}_{3x3} & \mathbf{K}_{g4} \end{bmatrix}, \quad \text{(A.3)}$$

$$\mathbf{K}_g^{22} = \begin{bmatrix} \mathbf{K}_{g5}^{11} & \mathbf{K}_{g5}^{12} & \mathbf{O}_{3x3} & \mathbf{O}_{3x3} \\ \mathbf{K}_{g5}^{21} & \mathbf{K}_{g5}^{22} & \mathbf{O}_{3x3} & \mathbf{O}_{3x3} \\ \mathbf{O}_{3x3} & \mathbf{O}_{3x3} & \mathbf{K}_{g6}^{11} & \mathbf{K}_{g6}^{12} \\ \mathbf{O}_{3x3} & \mathbf{O}_{3x3} & \mathbf{K}_{g6}^{21} & \mathbf{K}_{g6}^{22} \end{bmatrix}, \quad \text{(A.4)}$$

$$\mathbf{K}_g^{12} = \begin{bmatrix} \mathbf{K}_{a1} & \mathbf{K}_{a1}\mathbf{E}_{g5,a1} & \mathbf{K}_{m1} & \mathbf{K}_{m1}\mathbf{E}_{g6,m1} \\ \mathbf{K}_{a2} & \mathbf{K}_{a2}\mathbf{E}_{g5,a2} & \mathbf{K}_{m2} & \mathbf{K}_{m2}\mathbf{E}_{g6,m2} \\ \mathbf{K}_{a3} & \mathbf{K}_{a3}\mathbf{E}_{g5,a3} & \mathbf{K}_{m3} & \mathbf{K}_{m3}\mathbf{E}_{g6,m3} \\ \mathbf{K}_{a4} & \mathbf{K}_{a4}\mathbf{E}_{g5,a4} & \mathbf{K}_{m4} & \mathbf{K}_{m4}\mathbf{E}_{g6,m4} \end{bmatrix} = \left[\mathbf{K}_g^{21}\right]^T, \quad \text{(A.5)}$$

and $\mathbf{O}_{nxn}$ is an *n x n* null matrix.

APPENDIX B: LIST OF SYMBOLS

C	viscous damping matrix
$C_{\varphi i}$	$= \cos\varphi_{mi}^{x}$
E	skew symmetric matrix
F	control force amplitude vector
$\mathcal{F}$	complex control force amplitude
f	control force vector
f(*t*)	time varying control force
H	dynamic compliance matrix
i	square root of -1
I	mass moment of inertia
K	stiffness matrix
k	stiffness
ℓ	length
M	inertia matrix
m	mass
O	matrix of zeros
Q	generalized displacement amplitude vector
Q	generalized displacement amplitude
q	generalized displacement vector
q	generalized displacement
$\mathfrak{R}$	rotational transformation matrix
r	position vector
r	coordinates of position vector
$S_{\varphi i}$	$= \sin\varphi_{mi}^{x}$
T	torque excitation amplitude
$\mathfrak{T}(t)$	time varying torque excitation
W	disturbance excitation amplitude vector
W	disturbance excitation amplitude
w	disturbance excitation vector
w(*t*)	time varying disturbance excitation
x, y, z	Cartesian coordinates
Γ	Cartesian coordinate system
ε	translational displacement vector at center of mass
ε	translational displacement at center of mass
θ	rotational displacement vector
θ	rotational displacement
μ	proportional damping coefficients
ν	eigenvector
Π	transformation matrix
υ	directional cosine
φ	vector of Euler angles
φ	Euler angle
Ω	resonance frequency (rad sec^{-1})
ω	circular frequency (rad sec^{-1})

Subscripts

0,1,…,*n*	general indices
a	active powertrain mount
b	passive base (frame) mount
g	referenced to discrete inertia element coordinates
i	mount index
j	inertia index
m	passive powertrain mount
n x n	matrix of dimension (*n*, *n*)
ˆ	active path element modified to a passive element

Superscripts

T	transpose
x, y, z	referenced to Cartesian coordinates
ε	translational direction
θ	rotational direction
˜	complex valued
–	normalized
′	relating to inertial coordinates
″	relating to elastic coordinates

Operators

diag( )	diagonal matrix

Abbreviations

c.g.	center of gravity
TRA	torque roll axis